ELSEVIER

Polymer 43 (2002) 6005–6012

polymer

www.elsevier.com/locate/polymer

In situ study of nanostructure and morphological development during the crystal–mesophase transition of poly(di-*n*-hexylsilane) and poly(di-*n*-butylsilane) by X-ray and hot-stage AFM

Zhijun Hu, Binyang Du, Fajun Zhang, Fengchao Xie, Tianbai He*

State Key Laboratory of Polymer Physics and Chemistry, Changchun Institute of Applied Chemistry, Chinese Academy of Sciences, Changchun, Jilin 130022, People's Republic of China

Received 4 February 2002; received in revised form 7 May 2002; accepted 24 June 2002

Abstract

Nanostructure and morphology and their development of poly(di-*n*-hexylsilane) (PDHS) and poly(di-*n*-butylsilane) (PDBS) during the crystal–mesophase transition are investigated using small angle X-ray scattering (SAXS), wide angle X-ray diffraction and hot-stage atomic force microscopy. At room temperature, PDHS consists of stacks of lamellae separated by mesophase layers, which can be well accounted using an ideal two-phase model. During the crystal–mesophase transition, obvious morphological changes are observed due to the marked changes in main chain conformation and intermolecular distances between crystalline phase and mesophase. In contrast to PDHS, the lamellae in PDBS barely show anisotropy in dimensions at room temperature. The nonperiodic structure and rather small electronic density fluctuation in PDBS lead to the much weak SAXS. The nonperiodic structure is preserved during the crystal–mesophase transition because of the similarity of main chain conformation and intermolecular distances between crystalline phase and mesophase. © 2002 Published by Elsevier Science Ltd.

Keywords: Polysilane; Morphology; Crystal–mesophase transition

1. Introduction

Polysilanes are a relatively new class of polymers, containing linear Si–Si catenation in the main chain with two organic substituents at each silicon. The delocalization of σ-electrons along the silicon backbone leads to UV absorption as well as photoconductivity and semiconducting properties [1,2], similar to those of π-conjugated polymers.

One of the most exotic properties of polysilanes is their thermochromism [3]. Wide angle X-ray diffraction (WAXD) [4], vibrational spectroscopy [5–7] and ^{13}C and ^{29}Si NMR [8,9] has been used to investigate the structures associated with the electronic absorption bands in the solid state of poly(di-*n*-hexylsilane) (PDHS). The silicon backbone is in a *trans* planar zigzag conformation and the hexyl side chains are packed in an ordered *trans*-like array perpendicular to the silicon backbone at room temperature. As the temperature is raised above the crystal–mesophase transition temperature (42 °C), conformational defects are introduced into the backbone and the side chains undergo partial disordering. The change of main chain conformation gives rise to a very sharp and dramatic thermochromic transition in the solid state.

Though thermal and structural analyses of poly(di-*n*-butylsilane) (PDBS) show weak crystal–mesophase transitions at 85 °C, PDBS do not exhibit dramatic thermochromism in the solid state [10]. X-ray diffraction and ^{13}C and ^{29}Si NMR studies [10] showed that the crystalline structure of PDBS at room temperature was less ordered than that of PDHS and had quasi-hexagonal intermolecular packing. The backbone of PDBS forms 7/3 helices under ambient conditions, resulting in a blue shift of ca. 60 nm in UV absorption to that of the all-*trans* PDHS chain. The 7/3 helical conformation is changed to disordered structure above this crystal–mesophase transition temperature.

Although much progress has been made in the structural determination and thermochromism of polysilanes [3], less attention has been paid on their morphology, even less the morphological changes accompanying the crystal–mesophase transition. However, morphology plays a crucial role

* Corresponding author. Tel.: +86-431-5262-123; fax: +86-431-5262-126.

E-mail address: tbhe@ns.ciac.jl.cn (T. He).

0032-3861/02/$ - see front matter © 2002 Published by Elsevier Science Ltd.
PII: S0032-3861(02)00398-1

on the manipulation of physical properties of conjugated polymers and its knowledge is of utmost importance in any applications [11]. Thus, understanding the relationship between properties and morphology remains a challenge in polysilanes. Only preliminary results [12] on the morphology of polysilanes were obtained by use of optical microscopy. Such studies are limited by the resolving power and often by the overlaying of features in depth in the field of view. Transmission electron microscopy (TEM) provides excellent resolution and has provided most of morphological detail in melt-crystallized polymers. Wu et al. [13] provided the result on phase structure and morphology of a poly(methyloctadecylsilane) oligomer by TEM. However, because of beam damage to the specimen, TEM is effectively incapable of following the development of structure and morphology.

In the present work, the two typical dialkylsubstituted polysilanes, PDBS and PDHS, are chosen to study the nanostructure and morphology and their development during the crystal–mesophase transitions in situ by WAXD, small angle X-ray scattering (SAXS) and atomic force microscopy (AFM). The two polysilanes are chosen because of their different backbone conformation under ambient conditions and dissimilar solid state thermochromic transition.

2. Experimental section

2.1. Materials

PDHS and PDBS are prepared from the corresponding dichlorosilanes by dehalogenation coupling with sodium under standard conditions for polysilanes synthesis by Wurtz coupling reaction [14]. After purification from toluene with isopropyl alcohol (twice) and tetrahydrofuran with methanol, flocculent, pure white, oligomer-free samples of PDHS and PDBS are obtained. The molecular weight determined by gel permeation chromatography in tetrahydrofuran solution is $M_n = 1.2 \times 10^4$ ($M_w/M_n = 1.4$), and $M_n = 1.7 \times 10^4$ ($M_w/M_n = 1.8$), respectively.

2.2. Instruments

WAXD experiments are conducted with a Rigaku 18 kW rotating-anode generator (Cu Kα) with a diffractometer with $I = 200$ mA and $V = 40$ kV. The X-ray beam is monochromatized using a graphite crystal. The diffraction peak positions and widths are calibrated through silicon crystals with known crystal sizes. The 2θ angle region ranges between 2 and 40° with a scanning rate of 0.3°/min. Samples prior to use are heated well above the crystal–mesophase transition temperature and then cooled slowly to room temperature. The desired temperature of samples during scanning is controlled with a medium and low temperature attachment. The heating and cooling are performed in 10 °C step and the set temperature can be maintained to within ± 1.0 °C during scanning.

The SAXS experiments are carried out on a Philips PW1700 X-ray Diffractometer with Kraky small angle scatter system with $I = 40$ mA and $V = 45$ kV, Cu Kα ray. The distance between the sample and the detector is 20 cm. Monochromatization is achieved using a graphite crystal. The samples are pressed with thickness of about 0.5 mm at well above the crystal–mesophase transition temperature and then cooled slowly to room temperature. The temperature of samples is controlled with a thermal accessory. One can heat or cool a sample to the temperature of interest and keep it constant with an accuracy of ± 1.0 °C.

AFM studies are performed with a SPA-300HV AFM with a SPI 3500N controller (Seiko Instruments Industry Co., Ltd). The temperature varies between room temperature and 100 °C and is calibrated with gallium and indium. All experiments are carried out using dynamic force mode under ultra high vacuum ($< 10^{-4}$ Pa). Etched Si probes with resonant frequency of 250–300 kHz and spring constants of 42 N/m are used. The samples, which is pressed with thickness of about 0.1 mm at well above the crystal–mesophase transition temperature and then slowly cooled down to room temperature, are fixed on the puck of the heater with a metallic clamp from above. A small K-type thermocouple is inserted in between the clamp and the sample surface close to the scanning area and measures the sample temperature. The stability of the temperature of the sample is ca. ± 1.0 °C. The heating and cooling are performed in 5 °C step. When the temperature is changed, the tip is completely withdrawn from the surface and reengagement is performed after the sample temperature stabilizes.

3. Results and discussion

3.1. Nanostructures and their development of PDHS and PDBS in reciprocal space

SAXS reflects electron density fluctuations within a sample over a length range larger than the usual interatomic distances. SAXS from crystalline polymers can give rise to rather broad peaks. From the angular position of the maximum of the scattering, the long period, L, can be determined by application of Bragg's law. Fig. 1 represents the scattering curves of PDHS and PDBS under ambient conditions. A Bragg peak is found in the SAXS curve of PDHS, which clearly indicates that PDHS consists of periodically arranged crystalline lamellae separated by other phases in which the electronic density is different to that of the crystalline phase. In contrast, no Bragg peak can be observed in the scattering curve of PDBS.

To explain the obvious distinction between PDHS and PDBS, WAXD of the two samples are carried out upon heating and cooling. Fig. 2(a) and (b) shows the WAXD of

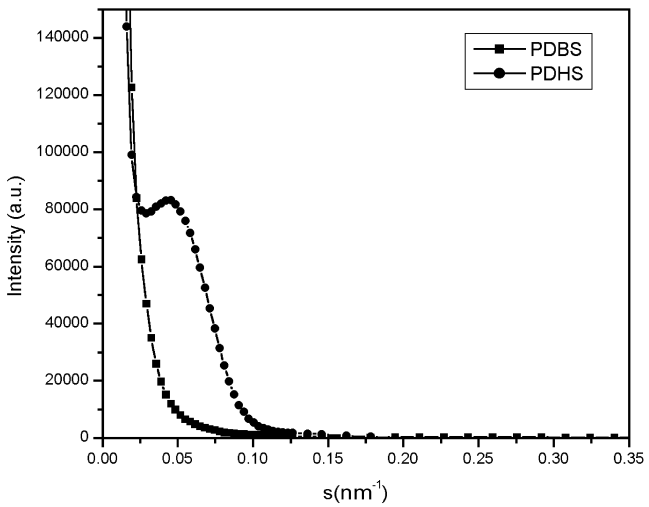

Fig. 1. SAXS curves of PDHS and PDBS at ambient conditions.

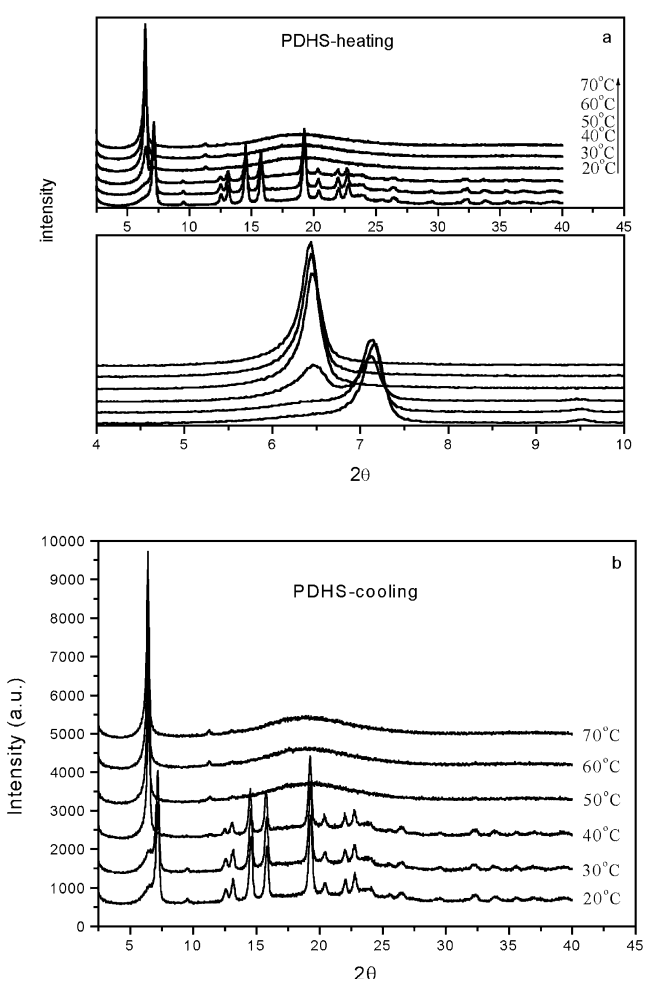

Fig. 2. Wide angle X-ray diffractograms of PDHS during (a) heating and (b) cooling. The bottom in (a) is the local part in the 4–10° 2θ range during heating.

PDHS during a heating and cooling cycle, respectively. For clarity, the diffraction curves are vertically shifted. Lovinger et al. [4] attributed all diffractograms at temperatures below that of the crystal–mesophase transition (42 °C) to two sets of superposed peaks. The first set includes all crystallographically sharp reflections centered at diffraction angles greater than 7.2°. The second set includes a broad peak at the smallest angle centered at 6.5° and the diffuse background beyond 12°. The first set of reflections is attributed to a crystallographically ordered phase, i.e. crystalline phase [4], and the second set is corresponding to mesophase [4,6]. It is reported that the backbone chain conformation in the crystalline phase was all-*trans* and the unit cell was orthorhombic with dimensions $a = 1.376$, $b = 2.386$ and $c = 0.399$ nm. The crystal lattice contained both silicon and alkyl side chain [15]. Though both main and side chains are randomized in the mesophase, the intermolecular order persists. The intermolecular packing was found to be hexagonal with unit cell dimension $a = 1.55$ nm [4]. The two strongest diffraction peaks centered at 7.2° for crystalline phase and 6.5° for mesophase represent the intermolecular packing of Si-backbone chains. The different intermolecular distances lead to the dissimilar density and then the electronic density between the two phases. If the two phases with different electronic density are arranged in an alternative manner, a Bragg peak should be observed in the SAXS curve as shown in Fig. 1.

Based on the two sets of diffraction peak area after background subtraction, the content of crystalline phase is estimated to be 80% at room temperature. As the temperature is increased from 20 to 40 °C, the diffraction intensities from crystalline phase continuously decrease accompanying with the increasing of the diffraction intensity from the mesophase, as shown in the bottom part in Fig. 2(a). Accordingly, the contents of crystalline phase reduce. Further heating to 50 °C or above, the diffraction intensity of mesophase rises sharply with the diminishing of reflection peak from crystalline phase. Subsequent cooling of the sample down to 20 °C, the crystalline structure and contents of crystalline phase are recovered, as shown in Fig. 2(b).

X-ray diffraction studies of PDBS indicate that the crystalline structure of PDBS is less ordered than that of PDHS. As shown in Fig. 3(a) and (b), the WAXD pattern is dominated by a strong reflection centered at 8.0°, which corresponds to the intermolecular distance [10]. The three weak peaks in the 19–22° range at ambient temperature are correlated to the intramolecular structure [10]. The observed changes of the crystalline structure of PDBS upon heating and cooling are very small and gradual, compared with the pronounced and discrete manifestations exhibited by PDHS at the crystal–mesophase transition. The peaks in 19–22° are replaced by a broad, amorphous-like background at temperatures above 80 °C, indicating randomization of the side chains. The intramolecular changes during the transition are reversible upon cooling as seen in Fig. 3(a).

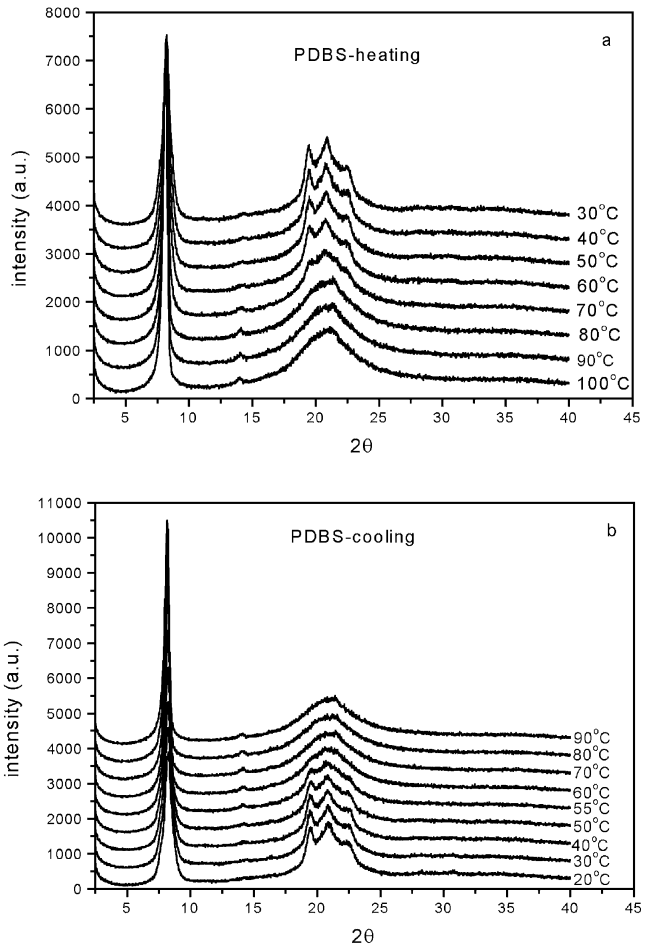

Fig. 3. Wide angle X-ray diffractograms of PDBS during (a) heating and (b) cooling.

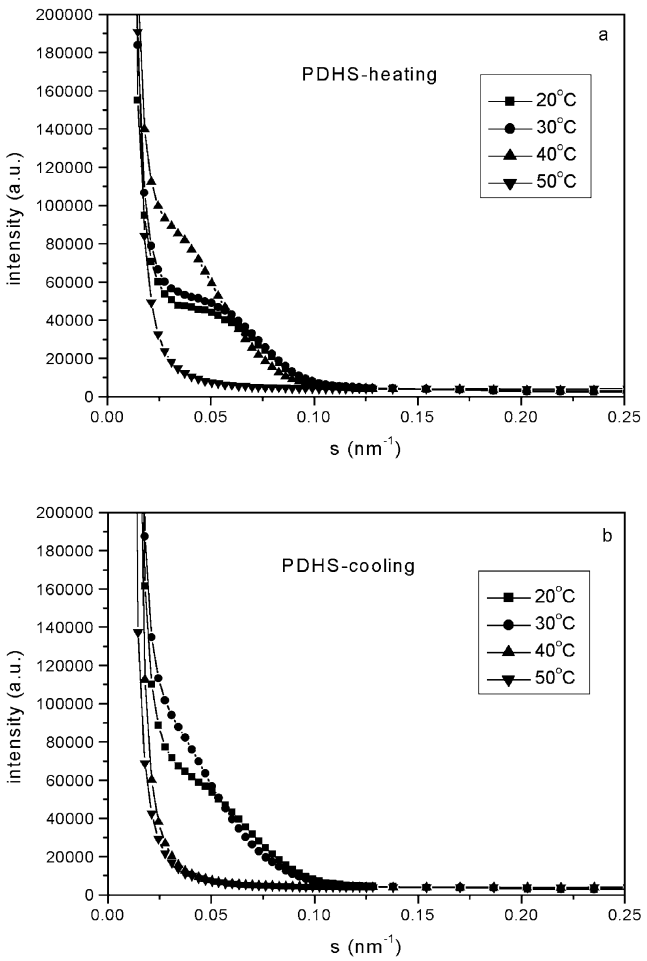

Fig. 4. SAXS curves of scattering intensity (in arb. units) versus scattering vector s for PDHS during (a) heating and (b) cooling.

As regards the intermolecular structure, Fig. 3(a) and (b) demonstrate that crystallographic packing is preserved at all temperatures, even above the disordering transition, which is in agreement with the earlier results of Schilling et al. [10]. In contrast to PDHS, there is no obvious change in either intermolecular distance or diffraction intensity between the crystalline phase and mesophase during the crystal–mesophase transition of PDBS because of the fairly similar conformation between the 7/3 helical and disordered conformation. The density and electronic density are too small to be concerned by SAXS. No Bragg peak is thus observed in SAXS curve. As expected, there is no obvious change in SAXS curves of PDBS during heating and cooling (data not shown).

Observed from the WAXD of PDHS, the content of crystalline phase changes with temperature during heating and cooling. Accordingly, Fig. 4(a) and (b) represents the SAXS curves of PDHS at different temperatures during heating and cooling, respectively. With increasing temperature the maxima of SAXS curves shift to smaller scattering angles, which corresponds to an increase of long period. Above the crystal–mesophase transition temperature, the maximum cannot be found, which clearly indicates the complete melting of crystalline lamellae in PDHS. Upon cooling, the maxima are observed again. The structural changes are reversible, but show a hysteresis between heating and cooling, which agree well with the results of WAXD as shown in Fig. 2.

The SAXS curves of PDHS can be interpreted based on an ideal two-phase model with alternating arrangement of crystalline lamellae and amorphous regions. The model assumes infinite lateral dimensions of the lamellae and hence it accounts the electron density change along the stacking direction (normal to the lamellae of the crystalline and amorphous boundary layers). Fig. 5 shows an electron

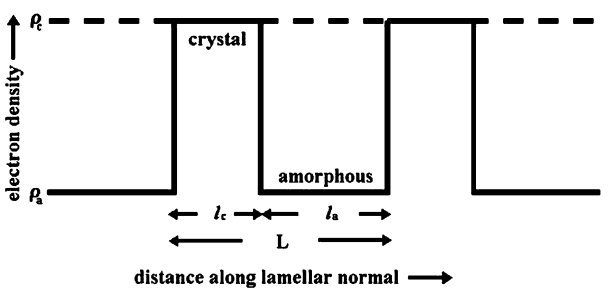

Fig. 5. Basic model for a lamellar stack.

density profile of a perpendicular section of a stack of alternating amorphous (electron density ρ_a) and crystalline (electron density ρ_c) layers, where the crystalline thickness, the amorphous thickness and total periodicity are indicated by l_c, l_a, and L, respectively.

Based on the ideal two-phase model, the morphological parameters can be directly evaluated from the one-dimensional electron density correlation function pioneered by Vonk [16], which can be obtained by Fourier transformation of the Lorenz corrected SAXS profiles

$$K(z) = \int_0^\infty s^2 I(s) \cos(2\pi sz)\mathrm{d}s \Big/ \int_0^\infty s^2 I(s)\mathrm{d}s \quad (1)$$

where s denotes the reciprocal space coordinate, $s = 2\sin\theta/\lambda$. $I(s)$ is the Lorentz corrected SAXS density.

The long period L can be estimated from the position of the first maximum L^M in the correlation function (Fig. 6). The thickness of the crystals, l_c, and that of the mesomorphic regions, l_a, and the linear degree of crystallinity X_c, $X_c = l_c/(l_c + l_a)$, may be computed from the correlation function $K(z)$ using the following relation [16]

$$\frac{B}{L^M} = X_c(1 - X_c) \quad (2a)$$

where X_c is defined by

$$l_c = X_c L^M \text{ and } l_a = (1 - X_c)L^M \quad (2b)$$

and B is the position of the first intercept of the correlation function with the abscissa. Note that Eqs. (2a) and (2b) are quadratic in X_c and can be solved to obtain two solutions for X_c. According to Babinet's principle, it is impossible to decide whether X_c corresponds to the mesomorphic or the crystalline phase. As demonstrated above, the crystalline fraction of PDHS at room temperature is well above 0.5. The linear degree of crystallinity of the sample at room temperature thus equals the larger value of X_c. At higher temperature, the crystallinity reduces and reaches 0.5. Beyond the temperature, the smaller value of X_c is taken as a measure for the degree of crystalline.

Fig. 6 shows the linear correlation functions obtained from the scattering curves represented in Fig. 4. One can observe different positions of the maximum of $K(z)$ corresponding to the different positions of the maximum in the scattering curves. The first maximum at ambient conditions is quite sharp, which reflects a relative high order of lamellar stacking. The peak significantly broadens at the vicinity of the transition temperature. Fig. 7 displays the evolution of L and l_c as a function of temperature during heating and cooling. As the sample is heated to 30 °C, both L and l_c do not change. At 40 °C, which is very close to the crystal–mesophase transition temperature, l_c decreases slightly, but L increases sharply. The simplest explanation is that besides the slightly disordering in the lamellar surface some full strand disordering also occurs [17]. Groups of crystalline lamellae or even complete stacks can disorder as a whole giving rise to larger mesomorphic regions. The reverse behavior during partial mesophase–crystal transition is observed. During cooling, the crystallization occurs at 30 °C. Further, on cooling to 20 °C very slight thickening of lamellae is observed, but the long period sharply decreases. The character of transitions is also shown by the change of crystallinity fraction as shown in Fig. 8. The morphological parameters at different temperature obtained from correlation functions are listed in Table 1.

One of the puzzling phenomena is that the changes in the average crystal lamellae are small compared to the shift of long period during the mesophase–crystal transition. The same phenomenon was observed [18] in polyethylene during melting and crystallization. Strobl et al. [18] suggested that decrease of the SAXS long period were brought about by the formation of the secondary population of thinner and more defective crystals. The explanation was confirmed by the multiple or broad melting peak appeared in

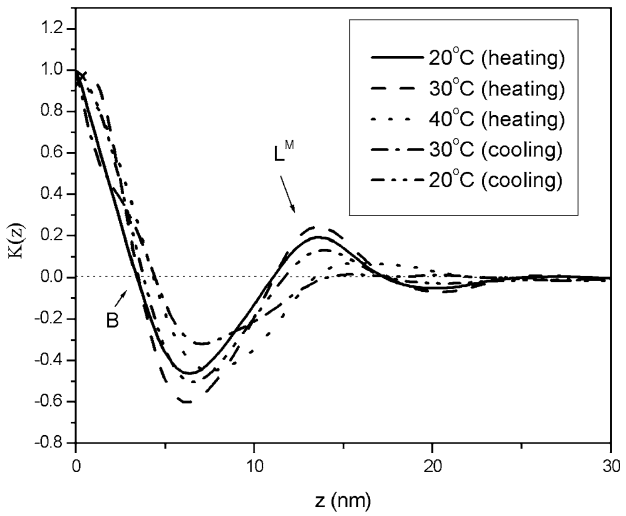

Fig. 6. Experimental correlation function obtained for PDHS during heating and cooling.

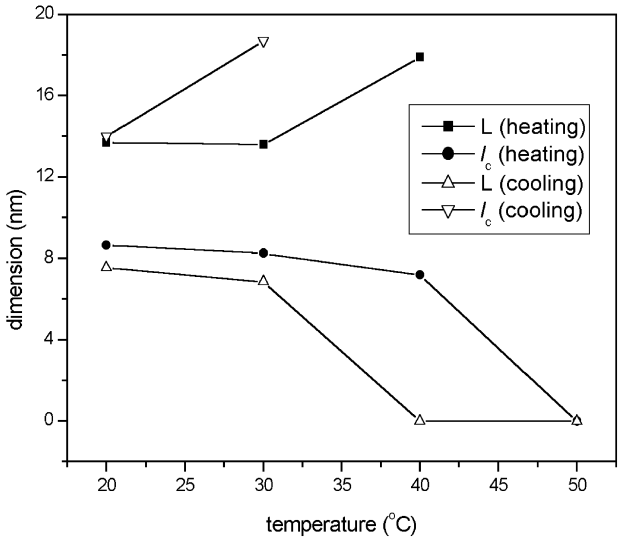

Fig. 7. Morphological parameters of the corresponding ideal two-phase structure of PDHS during heating and cooling.

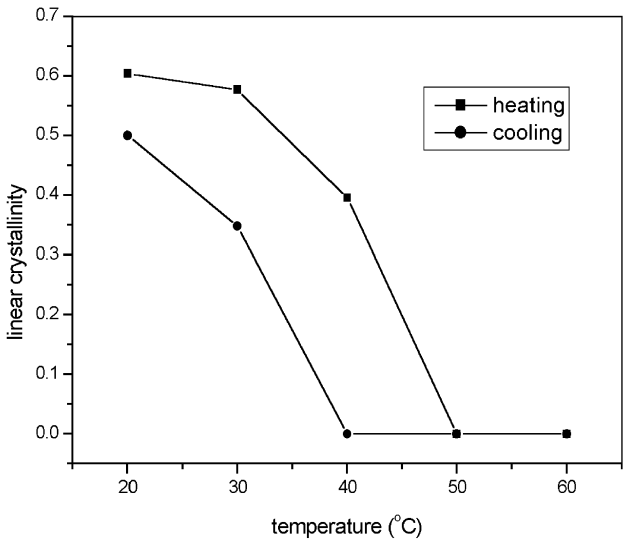

Fig. 8. The linear crystallinity of PDHS revealed by SAXS during heating and cooling.

endothermic curve of differential scanning calorimetry (DSC). Since only a sharp crystal–mesophase transition peak is observed in our DSC experiments of PDHS (data not shown), it is difficult to explain our experimental results using the model. Thus, we employ the hot-stage AFM to in situ observe the nanostructure and morphology evolution of PDHS during crystal–mesophase and mesophase–crystal transitions. On the basis of the AFM experimental results (see the next paragraph), the decreasing SAXS long period during mesophase–crystal transition can be explained by using the stack thickening process of lamellae.

3.2. Nanostructure and morphological development of PDHS and PDBS in real space

It has been reported [19] that AFM phase images can be correlated with the mechanical properties of polymer materials, such as stiffness, adhesion, etc. Phases recorded at moderate tapping are related to surface stiffness variations associated with Young's modulus change. Thus, AFM phase image can be used to distinguish the two phases of PDHS and PDBS and their development in situ.

The SAXS experiment is less sensitive to the nonperiodic structure, while AFM can provide information on this kind of morphological feature. Simultaneously obtained AFM height and phase data for PDBS at different temperatures are shown in Fig. 9. The total scan areas are 2000 nm × 2000 nm. The lamellae show organization into parallel orientations to differing degrees and barely show any anisotropy in dimensions at room temperature (Fig. 9(a) and (b)). The nonperiodic structure and rather small electronic density fluctuation of PDBS lead to the much weak SAXS as shown in Fig. 1.

Table 1
Summary of SAXS and AFM crystal dimensions of PDHS

Temperature (°C)	L_{SAXS} (nm)	l_c (nm)	L_{AFM} (nm)[a]	Length (nm)[b]
20[c]	13.7	8.6	12.9 ± 2.9	1000–7000
30[c]	13.6	8.3	14.1 ± 1.7	1000–7000
40[c]	17.9	7.2	52.8 ± 7.0	1000–7000
30[d]	18.7	6.9	13.2 ± 2.8	500–5000
20[d]	14.0	7.6	12.3 ± 2.3	500–5000

[a] L = spacing or long period between crystalline lamellae.
[b] Observed length of crystalline lamellae in the experiment ranges.
[c] During heating.
[d] During cooling.

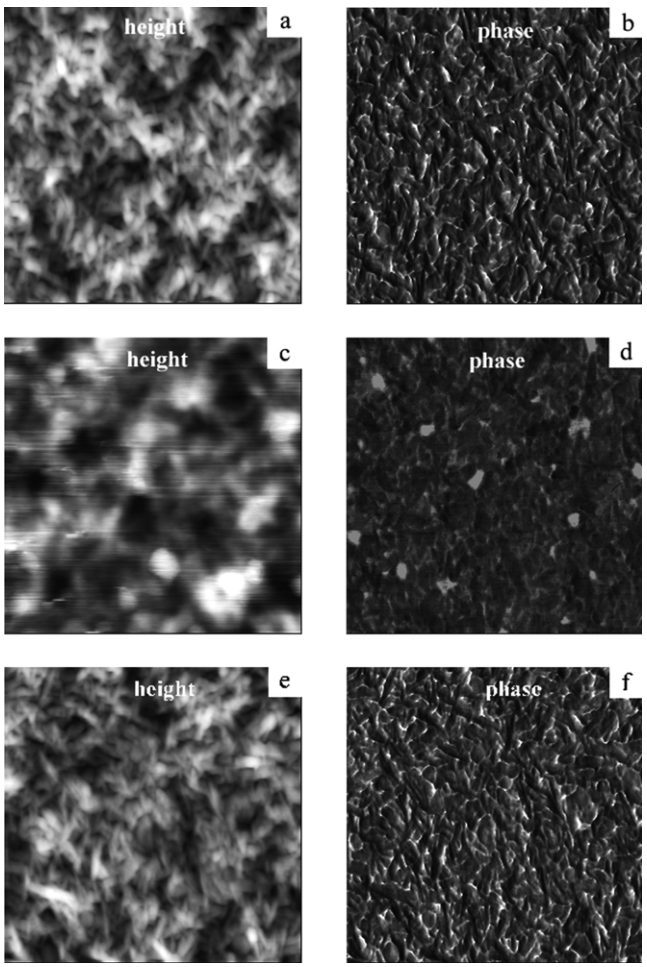

Fig. 9. Simultaneously recorded AFM height and phase images of PDBS during heating at (a,b) 20 °C; (c,d) 90 °C and (e,f) 20 °C. The contrast covers height variations in the 0–45 nm scale and phase variations in the −12–0°.

In step-like heating up to 90 °C, above the crystal–mesophase transition temperature, no critical morphological change is observed, as shown in Fig. 9(c) and (d). The lamellar morphology remains unchanged except structural details become less pronounced than that at room temperature. The results are reasonable since the main chain conformations between the crystalline phase and mesophase are similar [10] and the intermolecular distances are preserved during the crystal–mesophase transition as shown in Fig. 3. Upon cooling to room temperature, both

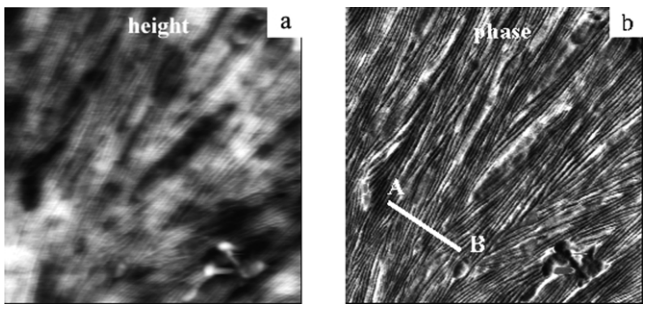

Fig. 10. AFM height and phase images of a surface of bulk PDHS. Images are recorded at room temperature. The contrast in the height image covers the surface corrugations in the 0–10 nm range and phase variations in the −12–0° range. The total scanning area is 1000 nm × 1000 nm.

height and phase images return to the original shape, as shown in Fig. 9(e) and (f).

Room temperature height and phase images of PDHS are shown in Fig. 10(a) and (b). Lots of nearly parallel lamellae, which are seen in both images, dominate the morphology of this sample. The sharp contrast between the lamellae and their surroundings in the phase image (Fig. 10(b)) indicates that the crystalline lamellae are stiffer than mesophase layers. One can assign the darker regions in phase image to crystalline lamellae, which are the higher parts in the corrugations in height image, and brighter regions to mesophase. The assignment is reasonable because the darker regions become obscure at elevated temperature and appear again after cooling to below the mesophase–crystal transition temperature (Fig. 12). Hence, the AFM images show that crystalline phase and mesophase coexist and they are periodically arranged in the sample of PDHS. The length of most lamellae is larger than 1 μm. A cross-section profile line between A and B shown in Fig. 10(b) is shown in Fig. 11. The lumpy shape is similar to the electron density profile of a perpendicular section of a stack of alternatively mesophase and crystalline layers as shown in Fig. 5. The average width of the corrugation is about 13 nm, which includes both the crystalline and mesophase regions.

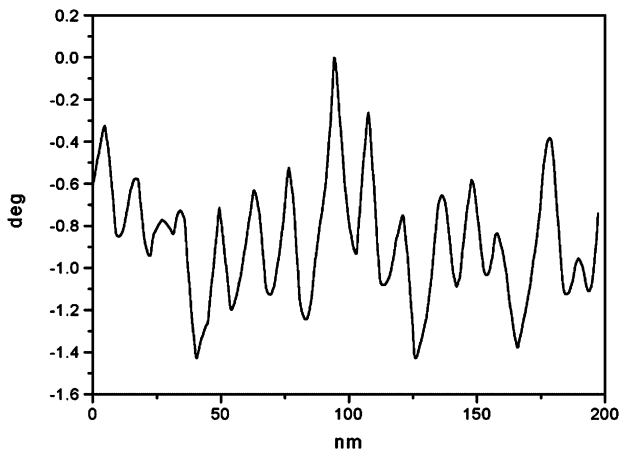

Fig. 11. The profile line of the cross-section between A and B shown in Fig. 10(b).

The crystalline lamellae are periodically arranged and separated by mesophase and the infinite lateral dimension of the lamellae compared with their width is in good agreement with the ideal two-phase model describing SAXS curves.

Though the character of this crystalline morphology of PDHS can be expected by SAXS, only AFM provides a direct visualization of the morphological development during the crystal–mesophase transition. In Fig. 12 can be seen a series of phase images of PDHS at different temperature at the same region as shown in Fig. 10. As shown in Fig. 12(a), in step-like heating up to 30 °C, the lamellar morphology remains unchanged, though structural details become less pronounced than at 20 °C (Fig. 10). Drastic morphology changes are found after heating to 40 °C. Fig. 12(b) shows that some of the lamellae disappear and the width of lamellae obviously increases, which is also consistent with increasing of the long period measured by SAXS. Further heating above the crystal–mesophase transition temperature, the morphology of the whole area become featureless, indicating the completely disordering transition of the crystalline lamellae (Fig. 12(c)).

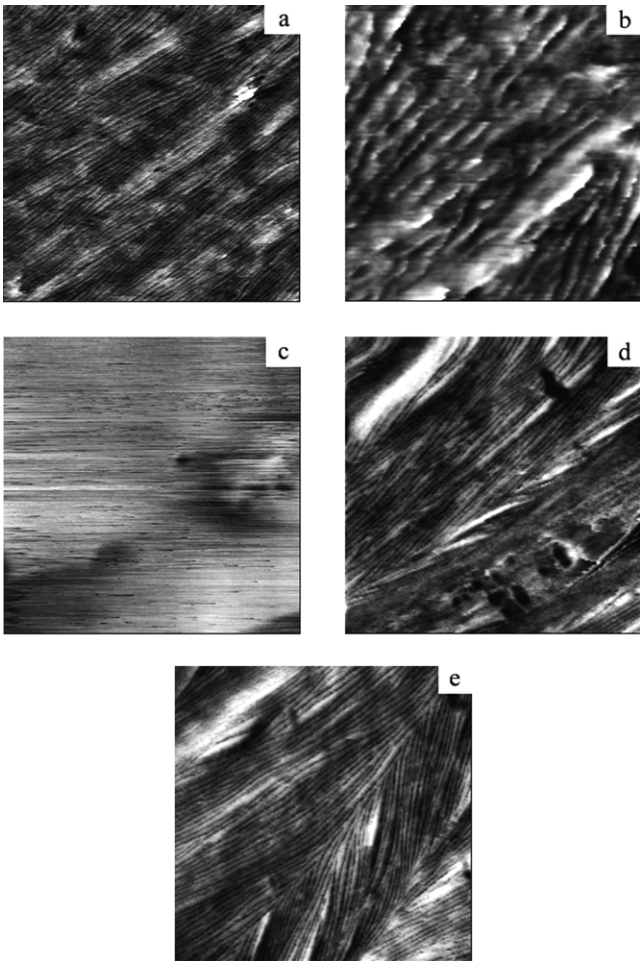

Fig. 12. (a–e) AFM phase images of PDHS during heating at (a) 30 °C; (b) 40 °C; (c) 50 °C, and cooling at (d) 30 °C; (e) 20 °C. The contrast of phase image is in the −12–0° range. The scanning area is 1000 nm × 1000 nm.

The morphological changes detected on cooling PDHS to room temperature reflect the ordering transition. The phase image obtained at 30 °C (Fig. 12(d)) exhibits numerous lamellae, which are embedded in the mesophase. The darker appearance of the lamellae in the phase image also confirms the assignment of the two phases. Further on cooling to 20 °C, some new stacks appear in the lower part of Fig. 12(e) and parallel lamellae in similar width add to the borders of already existing lamellae stacks at the right-hand corner. The phenomena clearly indicate that the decreasing of the SAXS long period during ordering transition must result from the thickening of the stacks of lamellae.

Compared with PDBS, the morphology changes in PDHS are critical during the crystal–mesophase transition. Note that the intermolecular distances in crystalline lamellae of PDHS change distinguishably during the crystal–mesophase transition, which results in the change of density. The change of density and main chain conformation lead to the variation of stiffness and then AFM phase images.

AFM data giving the lamellar dimensions at different temperature are listed in Table 1. The spacing or long period of lamellae is somewhat qualitative because of the unknown contributions of tip radii, tilting of lamellae under the surface, and various interface contributions. The values of L from AFM are approximately consistent with those from SAXS data (Table 1).

In short, for PDHS with a dramatic thermochromism in the solid state, there exists a critical structure and morphology change during the crystal–mesophase transition, while for PDBS with no dramatic thermochromism in the solid state, no critical morphology change has been seen.

4. Conclusions

The nanostructure and morphology and their development during the crystal–mesophase transition of PDHS and PDBS are studied in combined reciprocal space by means of SAXS, WAXD and in real space by AFM. At room temperature, PDHS consists of two phases, i.e. crystalline and mesomorphic phase. The crystalline lamellae are periodically separated by mesophase layers. The obvious difference of electronic density between the two phases leads to the Bragg peak in the SAXS curves. During the crystal–mesophase transition, the crystalline lamellae in PDHS convert to mesophase and obvious morphological changes are observed. PDBS shows somewhat different lamellae morphology, though the only difference between them is the length of side chains. The lamellae in PDBS show organization with different degrees of orientation and barely show any anisotropy in dimensions. The low anisotropy in dimensions and small electronic density fluctuation in PDBS result in quite weak SAXS. The nonperiodic structure in PDBS is preserved during the crystal–mesophase transition at elevated temperatures.

Acknowledgments

This work was supported by the National Science Foundation of China. We would like to thank Prof. Chengji Shan in Changchun Institute of Applied Chemistry for the assistance during synthesizing the samples.

References

[1] West R, David LD, Djurovich PI, Stearley KL, Srinivasan KSV, Yu H. J Am Chem Soc 1981;103:7352.
[2] Kepler RG, Zeigler JM, Havrah LA, Kurtz SR. Phys Rev B 1987;325:2818.
[3] Schilling FC, Bovey FA, Lovinger AJ, Zeigler JM. In: Zeigler JM, Fearon FG, editors. Silicon-based polymer science. Advances in chemistry 224, Washington, DC: American Chemical Society; 1990.
[4] Lovinger AJ, Schiling FC, Bovey FA, Zeigler JM. Macromolecules 1986;19:2657.
[5] Miller RD, Hofer D, Rabolt J, Fickes GN. J Am Chem Soc 1985;107:2172.
[6] Rabolt JF, Hofer D, Miller RD, Fickes GN. Macromolecules 1986;19:611.
[7] Kuzmany H, Rabolt JF, Farmer BL, Miller RD. J Chem Phys 1986;85:7413.
[8] Gobbi GC, Fleming WW, Sooriyakumaran R, Miller RD. J Am Chem Soc 1986;108:5624.
[9] Schilling FC, Bovey FA, Lovinger AJ, Zeigler JM. Macromolecules 1986;19:2660.
[10] Schilling FC, Lovinger AJ, Zeigler JM, Davis DD, Bovey FA. Macromolecules 1989;22:3055.
[11] Neher D. Adv Mater 1995;7:691.
[12] Yutaka M, Yasushi K, Yoshihiko N, Shuzi H. J Polym Sci, Part A: Polym Chem 1997;35:427.
[13] Wu Z, Xie F, Hu Z, Liu J, Du B, He T. Polymer 2001;42:1047.
[14] Trefonas P, West R. Inorg Synth 1988;25:58.
[15] Patnaik SS, Farmer BL. Polymer 1992;33:4443.
[16] Vonk CG, Kortleve G. Kolloid Z Z Polym 1967;220:19.
[17] Goderis B, Reynaers H, Koch MHJ, Mathot VBF. J Polym Sci, Part B: Polym Phys 1999;37:1715.
[18] Strobl GR, Schneider MJ, Voigt-Martin IG. J Polym Sci, Part B: Polym Phys 1980;23:1361.
[19] Magonov SN, Elings V, Whangbo MH. Surf Sci 1997;375:L386.